

Optimization of electrocoagulation process parameters for enhancing phosphate removal in a biofilm-electrocoagulation system

Zeng, Jie; Ji, Min; Zhao, Yingxin; Pedersen, Thomas Helmer; Wang, Hao

Published in:
Water Science and Technology

DOI (link to publication from Publisher):
[10.2166/wst.2021.132](https://doi.org/10.2166/wst.2021.132)

Creative Commons License
CC BY-NC-ND 4.0

Publication date:
2021

Document Version
Publisher's PDF, also known as Version of record

[Link to publication from Aalborg University](#)

Citation for published version (APA):
Zeng, J., Ji, M., Zhao, Y., Pedersen, T. H., & Wang, H. (2021). Optimization of electrocoagulation process parameters for enhancing phosphate removal in a biofilm-electrocoagulation system. *Water Science and Technology*, 83(10), 2560-2574. <https://doi.org/10.2166/wst.2021.132>

General rights

Copyright and moral rights for the publications made accessible in the public portal are retained by the authors and/or other copyright owners and it is a condition of accessing publications that users recognise and abide by the legal requirements associated with these rights.

- Users may download and print one copy of any publication from the public portal for the purpose of private study or research.
- You may not further distribute the material or use it for any profit-making activity or commercial gain
- You may freely distribute the URL identifying the publication in the public portal -

Take down policy

If you believe that this document breaches copyright please contact us at vbn@aub.aau.dk providing details, and we will remove access to the work immediately and investigate your claim.

Optimization of electrocoagulation process parameters for enhancing phosphate removal in a biofilm-electrocoagulation system

Jie Zeng, Min Ji , Yingxin Zhao , Thomas Helmer Pedersen  and Hao Wang


ABSTRACT

This study aimed to enhance the removal of phosphate in synthetic rural sewage by using a continuous electrocoagulation (EC) combined with biofilm process in an integrated system. Characteristic indexes of biofilm process effluent covering pH, dissolved oxygen (DO), suspended solids (SS), chemical oxygen demand (COD) and phosphate maintained a narrow fluctuation range and tended not readily to influence the phosphate removal of subsequent electrocoagulation. Three parameters including inter-electrode distance, current intensity and reaction time were selected to investigate the performance of enhancing phosphate removal. On the strength of single-factor tests, the Box-Behnken design (BBD) coupled with response surface methodology (RSM) was applied to investigate the individual and mutual interaction impacts of the major operating parameters and to optimize conditions. The optimum conditions were found to be inter-electrode distance of 1.8 cm, current density of 2.1 mA/cm² and EC reaction time of 34 min, and phosphate removal efficiency of 90.24% was achieved along with less than 1 mg/L in case of periodic polarity switching mode, which raised removal efficiency by 10.10% and reduced operating cost by 0.13 CNY/g PO₄⁻ compared to non-switching mode. The combination of biofilm processing and electrocoagulation treatment was proven to be a valid and feasible method for enhancing phosphate removal.

Key words | biofilm system, Box-Behnken design, combination, electrocoagulation, periodic polarity switching, phosphate removal

Jie Zeng

Min Ji 

Yingxin Zhao  (corresponding author)
School of Environmental Science and Engineering,
Tianjin University,
Tianjin 300350,
China
E-mail: yingxinzhao@tju.edu.cn

Thomas Helmer Pedersen 

Aalborg University, Department of Energy
Technology,
Pontoppidanstraede 111, DK-9220 Aalborg,
Denmark

Hao Wang

Tianjin Water Engineering Co., Ltd,
Tianjin, 300222,
China

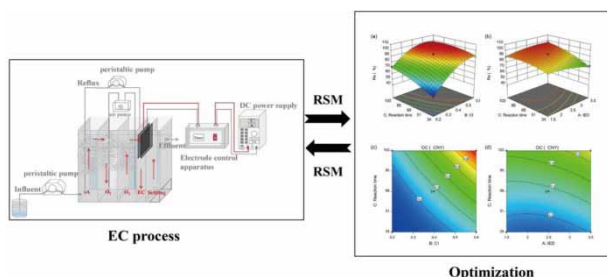
HIGHLIGHTS

- The combined biofilm and EC system was used to enhance phosphate removal.
- BBD was applied to optimize various operation parameters on phosphate removal.
- Phosphate removal of 90.24% was observed at optimal conditions.
- Utilization of periodic polarity switching achieved a better effect.

This is an Open Access article distributed under the terms of the Creative Commons Attribution Licence (CC BY-NC-ND 4.0), which permits copying and redistribution for non-commercial purposes with no derivatives, provided the original work is properly cited (<http://creativecommons.org/licenses/by-nc-nd/4.0/>).

doi: 10.2166/wst.2021.132

GRAPHICAL ABSTRACT

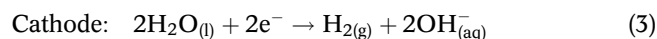
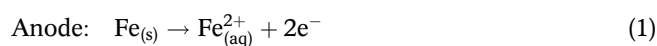


INTRODUCTION

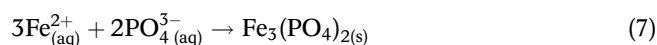
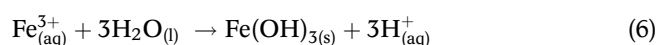
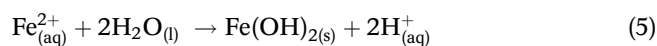
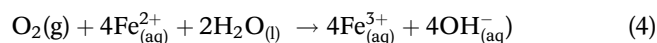
Currently, China has successively promulgated a series of stringent local standards for pollutants from rural sewage treatment facilities discharging into surface waterbodies, especially the indexes of the effluent phosphate. The excessive concentration of phosphate in water can cause eutrophication, leading to harmful ecological effects such as blooming toxic algae and depleting dissolved oxygen (DO) in the aquatic environment (Hashim *et al.* 2019). Besides, it may bring negative harm to human health such as loss of habitat (Bouwman *et al.* 2009). Rural sewage has the characteristics of small discharge and scattered distribution, intermittent discharge and relatively large volatility in water volume coefficient. Small integrated sewage treatment equipment is particularly well-suited for rural household sewage treatment due to its advantages of flexibility and small occupied area. As a typical nitrogen and phosphorus removal process, the Anoxic/Oxic (A/O) biofilm process has a preferable performance in denitrification, but a poor effect on the phosphorus removal, even less than 30% (Hosni *et al.* 2006). To solve this problem, the biological treatment usually has to be combined with other processes to further intensify the effluent quality to meet the discharge standards. Chemical coagulation-flocculation is the most common, such as casting ferric chloride or aluminum sulfate; however, there often exist certain disadvantages such as more complex process operation including extra dosing device and chemical reserve and large amount of sludge.

Electrocoagulation (EC), as a type of electrochemical technique, is proposed to be comparatively promising and effective for phosphate removal, during which an in-situ dissolution of submerged electrode takes place in the anode under the action of external voltage. Removal pathway of

phosphate can be summarized by several predominant chemical reactions below (Equations (1)–(8)):



Bulk solution:



In recent years, the combined biological and EC treatment mainly focused on the application of the simple EC process to treat effluent gained from biological treatment system (Buzzini *et al.* 2007; Damaraju *et al.* 2017), that is, researchers merely take treated water from biological process system as a feed to the EC process for advanced treatment, usually based on a batch EC treatment system (Yong *et al.* 2015). Also, the application of combined treatments has received vital interest for wastewater characterized by high chemical oxygen demand (COD) contents, color and heavy metals. A few attempts have been made involving integrated application of biofilm treatment followed by an EC process, particularly in enhancing phosphate removal. Although the combined system could reach

a decent removal efficiency and turned out to be technically feasible, the high operating costs, mainly including electrical consumption, and pollution issues in EC treatment have restricted more extensive large-scale applications of this combined treatment system. Consequently, the operation cost and the removal efficiency are two crucial targets that should be taken into consideration in assessing the overall properties of EC process, and it is essential to reduce overall operating cost together with enhancing effect of phosphorus removal by optimizing variables. These variables affect performance of the EC treatment, including phosphorus concentration, pH, DO, suspended solids (SS) and organic content from biofilm system effluent, reaction time, inter-electrode distance (IED), current intensity (CI), and electrode material (Attour *et al.* 2014; Kuokkanen *et al.* 2015; Dura & Breslin 2019a, 2019b). Traditional mathematical statistics methods, such as orthogonal method, cannot evaluate the interaction of various factors and then reflect the response relationship between influencing factors and target values. Response surface methodology (RSM), an optimizing statistical experimental design, has been successfully adopted for optimization of various biochemical processes (Bakshi *et al.* 2020). It can attain the aforementioned goal with the establishment of a sequential variable surface model, as well as predict the response of a system under a new condition (Tak *et al.* 2015). Box-Behnken design (BBD) only needs to consider factors at the mid-points of the edges and at the center without considering any other factorial points, so it requires fewer test groups compared with central composite design (CCD) (Almeida *et al.* 2008; Kabuk *et al.* 2014). Therefore, a BBD model is applied in this research to achieve a lower operating cost and a higher removal efficiency more quickly and reliably. Passivation often reduces active area of electrodes, and consequently increases ohmic resistance and the power consumed (Shonza *et al.* 2020). However, switching polarity contributes to the reduction of electrode passivation.

Accordingly, for the scope of this paper, a novel process system combining the biofilm system with EC treatment was proposed to enhance soluble phosphate removal. Three major parameters covering IED, CI and reaction time of EC were selected to investigate the performance of phosphate removal using periodic reversal polarity in the EC process. Based on it, BBD coupled with RSM was used to optimize these independent variables on phosphorus removal and operating cost as dependent variables. Meanwhile, the difference between the switching polarity and the non-switching polarity under the optimum conditions on operation was analyzed.

MATERIALS AND METHODS

Experimental materials

Synthetic rural sewage for this study was collected in a 50 L plastic bucket at laboratory scale with the addition of 9.4 g $C_6H_{12}O_6$, 7.6 g NH_4Cl , 2.2 g KH_2PO_4 and 13.75 g Na_2CO_3 . All chemicals were analytically pure. Its corresponding characteristics are pH of 7.4 ± 0.2 , COD of 190 ± 15 mg/L, nitrogen of 40.0 ± 1.8 mg/L, soluble phosphate of 10.0 ± 0.5 mg/L, bicarbonate alkalinity of 163.7 ± 10.2 mg/L $CaCO_3$ and conductivity of $1,178 \pm 102$ $\mu S/cm$.

Experimental set-up

Experimental set-up of integrated treatment system

Schematic diagram of experimental set up for integrated treatment system is given in Figure 1. As noted in the figure, the experiments were carried out in a cuboid plexiglass reactor of 42 cm length, 12 cm width and 38 cm height, with a volume of 21.282 L (working volume of 11.46 L, similarly hereinafter). The reactor consisted of two parts: one was biofilm reaction area, involving primary anaerobic area (A) of 3.36 L, two aerobic areas (O_1 and O_2) of 3.24 L each, and the other was EC unit (EC) of 1.62 L as well as sediment region (Settling) of 2.12 L. A composite filler composed of polypropylene (PP) spherical carrier outside and modified PP fiber inside was taken as carrier type, and the filling ratio was controlled at 50% for all zones. Reflux ratio from O_2 to A was maintained at 200%. The red arrow indicates the direction of water flow, and the baffling flow was achieved by overflow apertures on partition plate. The combined biofilm-EC system operated in a continuous flow mode, so the reaction time of EC tank can be controlled by adjusting hydraulic retention time (HRT) of the combined system. Rectangular electrodes made from iron (16 cm \times 12 cm) were used as cathode and anode, with an active surface area of 120 cm² in regard to submerged wetted area each, connected to a digital DC power supply (APS3005DM, 30 V/5A) in monopolar parallel connection and operated at galvanostatic mode. The electrode control apparatus was capable of periodically switching the polarity every 10 min. Prior to all electrocoagulation experiments, and in order to avoid an oxidation film, the electrodes were soaked in 1% HCl aqueous solutions for 30 min to remove superficial rust, then rubbed with 400 Grain Size abrasive paper and rinsed off by deionized

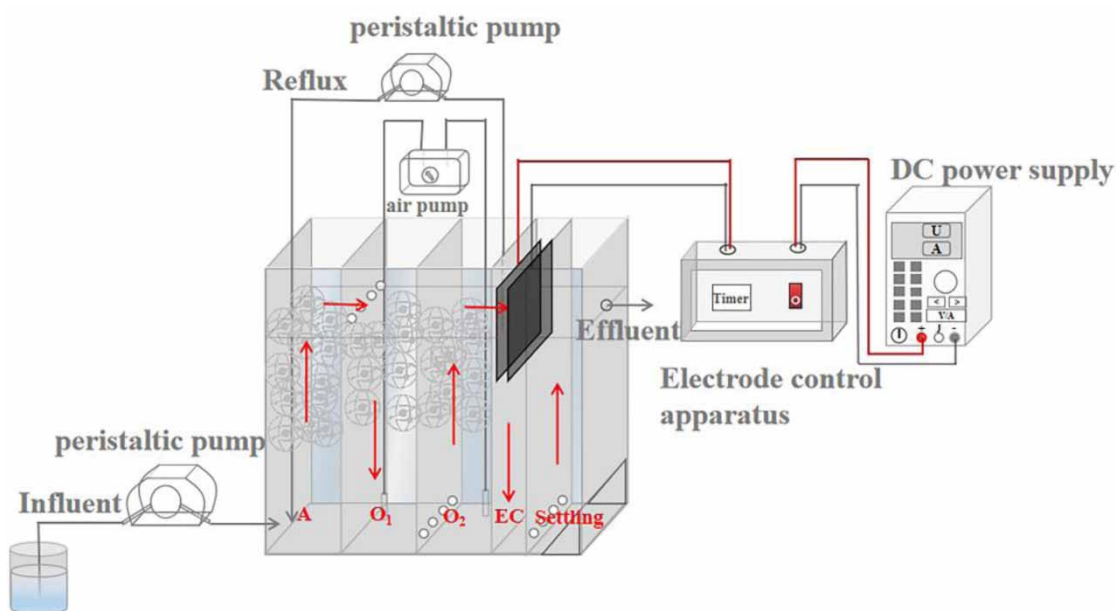


Figure 1 | Schematic diagram of the lab-scale set-up for enhancing phosphate removal.

water. Electrode plates were cleaned thoroughly with 1% HCl and tap water to remove the oxide layers at regular intervals.

During the tests, wastewater samples were collected after a total HRT (4, 8, 12, 16 h) of the combined system for the sake of reaching stabilization of removal effect. These samples were made to pass through 0.45 μm polyethersulfone (PES) syringe filters. Simultaneously, voltage values were recorded over time and the entire experimentation was preserved thermostatically at $26 \pm 1^\circ\text{C}$.

Experimental set-up of iron dissolution

The batch experiments of iron dissolution were conducted in a cuboid plexiglass reactor of 10 cm length, 12 cm width and 38 cm height, with effective volume of 1.92 L, equipped with a magnetic stirrer. Electrodes and the active surface area were the same as above. Also, the power supply mode was the same as above. To improve conductivity, 800 mg/L sodium chloride was added to tap water. Taken-out samples were added into a certain amount of (1 + 3) HCl (1 volume HCl + 3 volumes water) and then filtered for further analysis.

Analytical methods

COD and total iron were determined through direct reading spectrophotometer (DR/900, HACH, USA), and other

indicators were measured referring to the standard methods (APHA 1999), including SS, ammonia, nitrite, nitrate, and soluble phosphate. Solution pH and DO were monitored by a bench pH meter (METTLER TOLEDO, FE28, USA) and a dissolved oxygen meter (HACH, HQ30D).

The current efficiency was calculated based on the ratio of the theoretical iron dissolution rate and the actual iron dissolution rate. According to Faraday's Law, the calculation equation of the theoretical total iron dissolution rate (9):

$$v = \frac{m}{t} = \frac{60IM}{nFS} \quad (9)$$

where, v ($\text{mg}/(\text{min} \cdot \text{cm}^2)$) is the theoretical iron dissolution rate; m (mg/cm^2) is the mass of dissolved iron per unit area; I (A) is the current intensity; n is number of electron transferred ($z = 2$); F is Faraday's constant ($96,485 \text{ C/mol}$); M is molecular mass of iron and S is the effective area of electrode plate (120 cm^2).

The current efficiency (CE) was calculated with Equation (10):

$$CE = \frac{\text{Actual iron dissolution rate}}{\text{Theoretical iron dissolution rate}} \times 100\% \quad (10)$$

The removal efficiency (R) was calculated with the following Equation (11):

$$R = \frac{C_0 - C_i}{C_0} \times 100\% \quad (11)$$

where, R (%) is removal efficiency; C_0 (mg/L) is the initial soluble phosphate concentration and C_i (mg/L) is final soluble phosphate concentration in the EC cell.

A tech-economic operating cost was requisite for the EC process, which encompassed the loss of electrode materials and energy consumption as well as other indispensable expenses like maintenance cost (cleaning of the electrodes, chemicals, etc.) (Garg & Prasad 2016); nevertheless, the dominant operating cost was comprised of the first two aspects in the present study (Daneshvar et al. 2006).

Electrical energy can be calculated by using the relationship below (12):

$$E(\text{Wh/g}) = \frac{UI}{C_0QR} \quad (12)$$

where, E (Wh/g) is the electric consumption per weight of phosphate; U (V) is the average voltage; C_0 (mg/L) is the initial soluble phosphate concentration; Q (m³/h) is the rate of inflow and R (%) is removal efficiency.

The loss of electrode is deduced by the next equation according to Faraday's Law (13):

$$L(\text{g/g}) = \frac{3600IM}{nFC_0QR} \quad (13)$$

where, I (A), M (g/mol), C_0 (mg/L), n , F (C/mol) and Q (m³/h) were the same as above.

Consequently,

$$\text{Operating cost (OC)} = a \times E + b \times L \quad (14)$$

where, a is electrical cost (0.49 ¥, 2019) for 1 kWh and b is electrode cost obtained by the average China commercial market (4 ¥, 2019) per kilogram of iron.

Experimental design and data analysis

In this study, a three-factor three-level BBD matrix via Design Expert 10 software (StatEase, USA) was utilized to elucidate the individual and mutual interaction effects of three independent variables, IED (X_1), CI (X_2) and reaction time (X_3), while phosphate removal (Y_1) and OC (Y_2) were

chosen as target response functions. RSM coupled with BBD requires fewer test runs, owing to each variable being merely placed at one of three equally spaced values (Chauhan 2013) and not accounting for any fractional factorial points (Acharya et al. 2018). So for statistical calculations, the total number of test runs for the BBD matrix was summed up using the following Equation (15):

$$N = 2k(k - 1) + C_p \quad (15)$$

where, N is the number of experiments; k is the number of factors studied (k is equal to 3 here) and C_p is center points for assessing experiment error and running the model adequacy check (Makwana & Ahammed 2016).

The total designed experiments involved in 17 experimental runs with 5-fold repetition of center points were based on a BBD matrix at low, intermediate and high levels (−1, 0, 1) of independent parameters integrating with single-factor trial results, which were conducted to narrow the range of process variables. All experiments under various conditions were at least duplicated, which warranted a favorable repeatability, except for five replicates at center points. Table 1 lists the coded and experimental values of the independent variables. EC reaction times of 34, 68 and 102 min corresponded to flow rates of 47.75, 23.88 and 15.92 ml/min individually as well as total retention time of combined biofilm system and EC treatment of 4, 8 and 12 h, respectively.

The correlation between the phosphate removal efficiency (Y_1), OC (Y_2) and the set of independent variables (X_i , i is from 1 to 3) was triggered by a quadratic polynomial equation, as shown below (16) (Maran et al. 2014):

$$\hat{y} = b_0 + \sum_{j=1}^k b_j x_j + \sum_{j=1}^k \sum_{u \neq j}^k b_{ju} x_j x_u + \sum_{j=1}^k b_{jj} x_j^2 + \varepsilon \quad (16)$$

where, b_0 is constant; b_j is the linear coefficient; b_{jj} is the squared coefficient; b_{ju} is the cross-product coefficient; k is the number of factors studied and ε is the error.

Table 1 | Coded and actual values of the independent variables of the design for the overall EC tests optimization

Variables	Factor	Codes levels of variables		
		− 1	0	1
IED (cm)	X_1	1.5	2.5	3.5
CI (A)	X_2	0.2	0.4	0.6
Reaction time (min)	X_3	34	68	102

Pareto analysis of variance (ANOVA) and calculation of regression coefficient were performed in order to substantiate the adequacy of the proposed polynomial model. The 2D contour plots and 3D response surfaces were exhibited to identify the optimal region and to elucidate the interaction effects of variables for the proposed process (Acharya et al. 2018). After that, competence of the model equation for predicting the optimum response values was validated through running the optimal operating conditions.

RESULTS

Characteristics of EC influent

EC influent is essentially the effluent of biofilm treatment. The biofilm reactor system has been operating stably for 3 months before this study. The total nitrogen removal efficiency of $62.7 \pm 5.4\%$ was obtained and effluent ammonia nitrogen retained at 6.8 ± 2.4 mg/L at the HRT of 12 h. However, the effect of phosphorus removal was significantly worse, since biological phosphorus removal mainly relies on the discharge of surplus sludge, and the amount of sludge discharged from biofilm treatment is relatively small. As can be seen from Table 2, the soluble phosphate concentration of biofilm process effluent was basically stable around 9 mg/L. Therefore, the EC tank was set up to enhance phosphate removal of effluent from biofilm system.

The characteristic indexes of EC cell influent are depicted in Table 2. Components of Fe flocs are very complex and the transformations of Fe(II) and Fe(III) are affected by DO. Different forms of iron compounds directly affect the removal efficiency of phosphate by EC. Meanwhile, excessive DO will participate in the cathode reaction, which will affect the amount of bubbles produced by the cathode and also affect the EC operation; therefore, DO of EC cell influent was also measured. The nitrogen removal effect of biofilm system under different EC reaction times was different. The ammonia and nitrate contents were 22.6 ± 1.1 and $3.1 \pm$

1.2 mg/L, respectively, at the EC reaction time of 34 min, and the ammonia and nitrate contents were 6.0 ± 1.6 and 7.4 ± 2.1 mg/L, respectively, at 136 min. This variation had little effect on follow-up EC phosphate removal, and further research has not been carried out in this paper.

Simultaneously, the effluent of biofilm process was comparatively clean, the fluctuation range of the above-mentioned indicators was narrow, and other indicators tended not to affect the EC process in phosphorus removal. Therefore, the combination of two processes was quite appropriate. Notably, the purpose of this study is to provide a reference for real sewage treatment, so the combined processes for real sewage treatment in this paper require further study. Considering that most pollutants and SS are removed by A/O process, their effects on operation were not considered in this study.

Iron dissolution under different factors

As can be observed from the equations of soluble phosphate removal pathway, it is directly related to the actual iron dissolution rate, and the current efficiency affects the actual iron dissolution rate. The actual change rate of iron concentration could be obtained by linear fitting between total iron concentration and reaction time (Supplementary Figure 1), and the effective volume of set-up was 1.92 L, from which the actual iron dissolution rate could be calculated. As CIs were 0.2, 0.3, 0.4, 0.6 A, the actual change rates of iron concentration were 0.23, 0.90, 2.83 and 4.99 mg/(L · min) (Supplementary Figure 1(a)), respectively, so the actual iron dissolution rates were 1.84×10^{-3} , 7.17×10^{-3} , 2.26×10^{-2} and 3.99×10^{-2} mg/(min · cm²). The corresponding current efficiency could be calculated as 12.71%, 33.02%, 78.13% and 91.94% (Supplementary Table 1), respectively. Compared with IED and reaction time, CI had a greater impact on the current efficiency, and this showed a significant increase with the increase of CI. This was explained by bubbles produced by the cathode gradually increasing as CI increased, so the polarization phenomenon was relieved, since the solution was fully mixed, which promoted the current efficiency. In turn, it was conducive to the iron dissolution and phosphate removal. Therefore, current efficiency should be noted when selecting the right parameter range for EC system.

Single-factor tests analysis

Effect of inter-electrode distance

It is well acknowledged that the efficiency of EC units is influenced by the IED. To assess its impact on phosphate

Table 2 | Characteristics of EC cell influent

Indexes	Values
pH	6.75–7.59
DO (mg/L)	3.8–5.5
SS (mg/L)	8–26
COD (mg/L)	6–24
Soluble phosphate (mg/L)	8.8–9.8

removal in a continual operation, a range of tests were controlled at four diverse IEDs (0.5, 1.5, 2.5 and 3.5 cm), an identical CI of 0.4 A and EC reaction time of 68 min.

The results obtained can be seen in Figure 2(a). It was noteworthy that it has emerged that formerly there was a gradually upward tendency, achieving 92.78% of maximum phosphate removal efficiency at 2.5 cm. Iron dissolution rate reached a maximum of $0.0226 \text{ mg}/(\text{min} \cdot \text{cm}^2)$ at 1.5 cm. The results from the present study were consistent with Zhang et al. (2013), in which total phosphorus (TP) removal efficiency increased with increasing the electrode gap from 1.5 to 2.5 cm, and then it decreased with further increase in the IED. A greater upwards flux is generated due to the fact that the amount of bubbles increases and their size decreases under a small IED, and it will make the iron hydroxide float from the solution to the surface of solution, reducing the contact opportunity between the iron hydroxide and phosphate in the solution (Zhang et al. 2013). The removal rate of phosphorus was the lowest when the IED was 0.5 cm, which might be due to the relatively large overpotential generated by concentration polarization. Given that average voltage was 12.76 V for 3.5 cm and 5.50 V for 0.5 cm, if it followed Ohm's law, the result would be 1.82 V for 0.5 cm. Therefore, a maximum overpotential occurred at the IED of 0.5 cm. At the same time, it could be obviously observed that there existed an approximately 2 cm thick layer of floc between the two plates for 0.5 cm, and thus the fluidity of the solution surface deteriorated intangibly, reducing the effective contact area between plates and liquid. When the electrode spacing was 3.5 cm, the removal rate of phosphorus decreased. Moreover, it could be seen that the amount of bubbles

abated and more iron oxides were formed at the anode surface as the IED increased. This phenomenon can be explained by the fact that a wider gap increases the mass transfer resistance of the solution. The hydrogen ions move to the cathode at a slower rate and the dissolved iron ions cannot leave the anode in time. Therefore, the iron ions as effective coagulants are more easily oxidized to form iron oxides, attaching to the anode, which in turn reduces iron dissolution rate. Comprehensively considering current efficiency and phosphate removal efficiency, IED in the range of 1.5–3.5 cm was exploited.

Ohmic drop arising from the ohmic resistance of the cell Ω , which can be expressed as Equation (17), will rise when IED increases, which in turn augments power consumption.

$$\Omega = \frac{X_1}{S \delta} \quad (17)$$

where, X_1 is the IED, S the electrode surface area and δ the conductivity. Thus, as can be apparently noticed from Figure 2(a), energy consumption increases from 0.190 to 0.413 (kWh/g (PO_4^-)) with the gap between electrodes growing from 0.5 to 3.5 cm, respectively.

Effect of current intensity

Current intensity is a pivotal parameter which affects the removal of phosphate in the EC technique. For the sake of estimating the effect of current intensity on phosphate removal efficiency, four different current intensities (0.2, 0.3, 0.4 and 0.6 A) were implemented under constant conditions of IED of 1.5 cm and EC reaction time of 68 min.

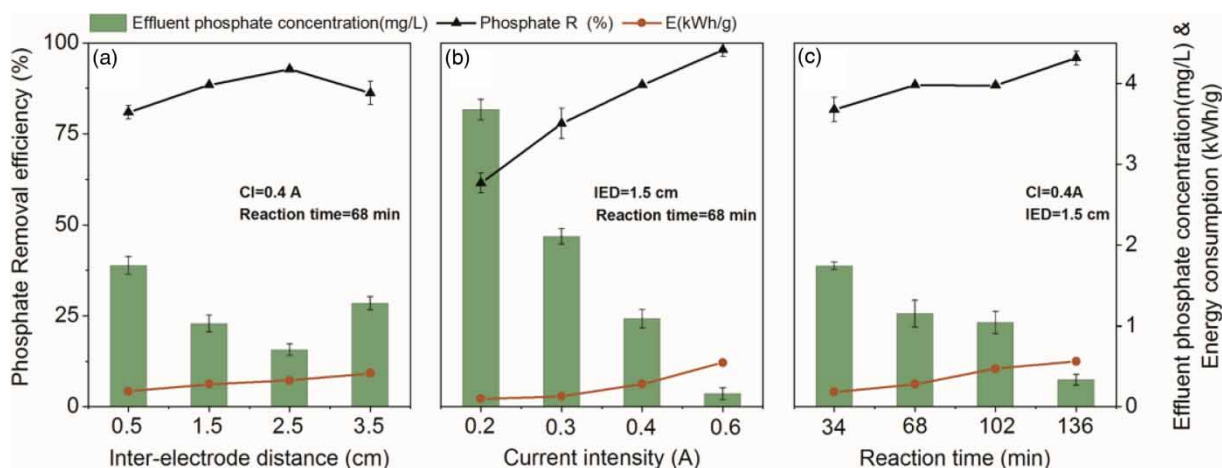


Figure 2 | Variation of phosphate removal and electrical cost as a function of various parameters: inter-electrode distance (a), current intensity (b) and reaction time (c).

The results are given in Figure 2(b). As can be observed, there was an increase of phosphate removal efficiency with rising current intensity to 0.6 A. This result corresponds to many previous studies (Xiang-yong *et al.* 2009; Castañeda *et al.* 2020), and it can be accounted for by Faraday's law that total iron dissolution rate significantly increased from 0.0018 to 0.0399 mg/(min · cm²) as CI increased from 0.2 to 0.6 A. Iron dissolution rate directly determines the amount of free iron and iron flocculant produced and then causes an increase in phosphate removal from 61.47% to 98.11%. Through measuring pH under different current intensities, it was found that the variation of pH was similar to that of current intensity and the current intensity of 0.2, 0.3, 0.4 and 0.6 A corresponded to pH of 7.2, 7.4, 7.8 and 8.3, respectively. It had been discovered that pH was linked to the conversion of iron to oxides and hydroxides and in turn affected the removal of phosphate. Meanwhile, it was interesting that there was less sludge at the bottom of the EC cell and more flocs suspended at a high current intensity. The reason lay in a faster production of H₂ bubbles as current intensity increased, enhancing the flotation capacity of suspended solids and colloids in water.

From another point of view, higher current intensity means higher consumption of electric energy required, which varies with the square of the CI and releases heat conforming to Joule's law (Amour *et al.* 2015), as presented in Figure 2(b), from approximately 0.08 to 0.545 (kWh/g (PO₄⁻)) as CI increased from 0.2 to 0.6 A. What is more, overdosing iron will as well also reverse the charge of settled particles, thereby sparking off them stable again and back-mixing of those to solution, which is not conducive to phosphorus removal and detrimental to electrode lifetime (Hakizimana *et al.* 2017). Overall, considering the current efficiency and OC, it might be reasonable to figure out that 0.4 A was an appropriate value for the rest of the experiments.

Effect of EC reaction time

For studying the impact of EC reaction time, experiments were accomplished with different reaction times of EC process (34, 68, 102, and 136 min). In order to lessen the test numbers of follow-up RSM optimization, ID was chosen as 1.5 cm and the remaining variables kept at 0.4 A. Results shown in Figure 2(c) revealed a positive correlation as EC reaction time increased from 34 to 136 min with a maximum removal efficiency of 95.83%, except that removal efficiency at 68 min had a narrow margin with that at 102 min. Likewise, Fe dissolution rate was positively related to EC reaction time, but it slightly fell when reaction

time was extended to 136 min. It is universally established that lower reaction time reduces opportunity for electrocoagulation, given that there was an ineffective and insufficient contact between phosphate present in the aqueous solution and the metal hydroxides produced.

Increasing EC reaction time dramatically boosted energy consumption; Figure 2(c) demonstrated that power consumption at a reaction time of 136 min was more than three times what it was at 34 min, 0.177 and 0.561 (kWh/g (PO₄⁻)) apart. Distinctly, redundant EC reaction time strikingly accelerated energy losses. As a consequence, a range of reaction time 34–102 min was elected in the RSM.

Model development and its validation

RSM model fitting and statistical analysis

RSM coupled with BBD was employed to explore the individual and mutual effect of process variables on phosphate removal. According to BBD, 17 statically designed test runs and their results are depicted in Table 3.

Then the BBD experimental data were analyzed by two sorts of fit summary, encompassing model summary statistics and the sequential model sum of squares, selecting the fittest model available to clarify the phosphate removal process. It was found that the quadratic model expresses the highest effectiveness ascribed to its high R², adjusted-R², predicted-R², F-value, and low *p*-value by contrast with linear and two-factor interaction (2FI). As a result, the quadratic model was used to obtain predicted values of the responses. In addition, the cubic model was aliased. The predicted values of the responses were gained from the quadratic model for the percentage of phosphate removal and operating cost. The response functions with the determined coefficients in terms of coded variables are given below (18) and (19):

$$Y_1(\%) = 92.38 - 1.28X_1 + 7.49X_3 + 0.68X_1X_2 + 47.8X_1X_3 - 4.05X_2X_3 - 2.78X_1^2 - 11.86X_2^2 - 3.77X_3^2 \quad (18)$$

$$Y_2(\text{CNY/g}) = 0.28 + 0.04X_1 + 0.16X_2 + 0.15X_3 + 0.03X_1X_3 + 0.03X_1^2 + 0.02X_2^2 + 0.03X_3^2 \quad (19)$$

where, the positive coefficients imply synergistic effects, whereas the negative coefficients antagonistic effects (Abbasi *et al.* 2020).

Table 3 | Statically designed test runs

Run	Independent variables (X_i)			Response (Y_i)			
	X_1 (cm) IED	X_2 (A) CD	X_3 (min) Reaction time	Experimental		Predicted	
				Phosphate removal (Y_1 , %)	Operating cost (Y_2 , CNY/g)	Phosphate removal (Y_1 , %)	Operating cost (Y_2 , CNY/g)
1	1.5(–)	0.2(–)	68(0)	61.47	0.14	61.97	0.12
2	3.5(+)	0.2(–)	68(0)	56.00	0.22	58.05	0.24
3	1.5(–)	0.6(+)	68(0)	98.11	0.44	96.06	0.45
4	3.5(+)	0.6(+)	68(0)	95.37	0.52	94.87	0.54
5	1.5(–)	0.4(0)	34(–)	84.37	0.16	84.39	0.25
6	3.5(+)	0.4(0)	34(–)	73.80	0.20	72.27	0.21
7	1.5(–)	0.4(0)	102(+)	88.29	0.43	89.82	0.43
8	3.5(+)	0.4(0)	102(+)	96.83	0.58	96.81	0.57
9	2.5(0)	0.2(–)	34(–)	48.00	0.10	47.48	0.10
10	2.5(0)	0.6(+)	34(–)	89.00	0.28	91.03	0.28
11	2.5(0)	0.2(–)	102(+)	72.60	0.22	70.57	0.21
12	2.5(0)	0.6(+)	102(+)	97.40	0.74	97.92	0.74
13	2.5(0)	0.4(0)	68(0)	92.78	0.28	92.38	0.26
14	2.5(0)	0.4(0)	68(0)	93.50	0.27	92.38	0.28
15	2.5(0)	0.4(0)	68(0)	94.20	0.29	92.38	0.28
16	2.5 (0)	0.4(0)	68(0)	90.40	0.26	92.38	0.28
17	2.5(0)	0.4(0)	68(0)	91.00	0.31	92.38	0.28

The ANOVA tests were performed as the authentication of statistical validation of the chosen model, and their results are listed in Table 4 (Design Expert 10).

F-value and P-value: To determine how well the parameters describe the variation in the mean of data, Fisher distribution (F-test) was used to validate the feasibility of the regression model. High F-values of 91.28 and 103.14 (Table 4) for R and OC, respectively, stated clearly the predictability of the model at the 95% confidence interval and only a 0.01% chance that it could occur due to noise. P-value is computed to judge whether the association among the response, each variable and their mutual interaction in the model is statistically significant, which is identified as the smallest level of significance conducive to rejection of the null hypothesis (Demim et al. 2014). P-values less than 5% suggest that model terms are significant. In this case, these terms, except for X_1 (IED) and X_1X_2 (the interaction effects of IED and CD) for R along with X_1X_2 and X_2^2 (square of CD) for OC, are significant terms. Lack of fit (LOF) as a comparative analysis between the residual error and the pure error from the designed central points is supposed to be insignificant. From Table 4 it is noted that the p-values for LOF regardless of R or OC are more than

5%, showing their insignificance (Makwana & Ahammed 2016).

Coefficient of variation (CV) and adequacy precision (AP): CV is the measure of the degree of dispersion of probability distribution, defined as the ratio of the standard error to the mean value of experimental response. When the CV is not exceeding 10%, the model is considered reproducible. In this study, plainly both CVs (Table 5) were below 10%. Adequacy precision, a measure of the signal to noise ratio (S/N), examines the range of the predicted responses relative to the error, along with a ratio (>4) deemed to be satisfactory for the modelling agreement. Easily witnessing, it is easily seen that the ratios were found to be 30.32 and 37.12 for responses, disclosing adequate signals.

R^2 , adjusted R^2 and predicted R^2 : large values (close to 1) of R^2 , adjusted R^2 and predicted R^2 are regarded as the suitability of a regression model. They were 0.9916, 0.9807 and 0.9039 for phosphate removal efficiency and 0.9925, 0.9829 and 0.9265 for OC, enough to validate the model. High R^2 , as the parameter to ensure a favorable correlation between experimental and predicted values, was obtained (Makwana & Ahammed 2016). Further, values of R^2 , adjusted R^2 and predicted R^2 should be in reasonable agreement with each

Table 4 | ANOVA results for quadratic model (Design Expert 10)

Source	R (%)					OC (CNY/g)				
	Sum of Squares	Mean Square	F-value	p-value		Sum of Squares	Mean Square	F-value	p-value	
Model	3,864.7	429.41	91.28	< 0.0001	significant	0.46	0.05	103.14	< 0.0001	significant
A-IED	13.11	13.11	2.79	0.1390		0.02	0.02	31.02	0.0008	
B-CI	2,513.8	2,513.76	534.33	< 0.0001		0.21	0.21	428.00	< 0.0001	
C-Reaction time	449.25	449.25	95.49	< 0.0001		0.19	0.19	383.15	< 0.0001	
AB	1.86	1.86	0.40	0.5491		0.00	0.00	0.00	1.0000	
AC	91.30	91.30	19.41	0.0031		0.00	0.00	6.13	0.0425	
BC	65.61	65.61	13.95	0.0073		0.03	0.03	58.55	0.0001	
A ²	32.61	32.61	6.93	0.0338		0.00	0.00	6.57	0.0374	
B ²	591.80	591.80	125.80	< 0.0001		0.00	0.00	3.50	0.1036	
C ²	59.86	59.86	12.72	0.0091		0.00	0.00	9.15	0.0193	
Residual	32.93	4.70				0.00	0.00			
Lack of Fit	22.38	7.46	2.83	0.1705	not significant	0.00	0.00	1.78	0.2901	not significant
Pure Error	10.55	2.64				0.00	0.00			
Cor Total	3,897.6					0.46				

Table 5 | Fit statistics for summarized model

	R	oc
Std. Dev.	2.1690	0.0222
Mean	83.7129	0.3200
CV %	2.5910	6.9400
R ²	0.9916	0.9925
Adjusted R ²	0.9807	0.9829
Predicted R ²	0.9039	0.9265
Adeq Precision	30.3210	37.1202

other (Jensen 2017). For two responses, R², adjusted R² and predicted R² do not differ considerably, and these are less than 0.2.

Variable interaction and response

Single-factor impact (linear and curvature) on removal efficiency and operating cost (responses) can be scrutinized by One Variable At A Time (OVAT) with ease, while the multi-factor interactions are characteristic paradigms of RSM analysis. Thus, the 3D response surface plots easily perceiving two-factor relations were created using the developed model graphs and displayed in Figure 3, where the red

region (sectors demarcated by orange arcs on the gray plane) is considered to reach the higher phosphate removal efficiency and the blue region represents the lower operation cost. Figure 3(a) presents interaction effects of reaction time and current intensity on phosphate removal efficiency, while the third factor was fixed at the center point. It could be inferred that the red region from the left exhibited the highest removal efficiency. As CI shifted towards 0.6 A, there was a comparable increase in phosphate removal at any given reaction time, which was ascribed to the fact that CI predominated in the disengagement rate of iron ions, yet reaction time showed curvature where phosphate removal had its peak value in the vicinity of 68 min of reaction time and further increase produced a dip in removal efficiency, whereas CI and reaction time (Figure 3(c)) unfolded collaborative effects, thereby magnifying operating cost by extending to the ends of the graphical axes. In the view of the interactive effect of reaction time and IED (Figure 3(b)), diagrammatically a similar variation tendency of phosphate removal efficiency was shared between reaction time and IED, where an increment primarily and decrement afterwards occurred. The behavior in 2D counter plot (Figure 3(d)) could be simply certified by Joule's Law, herein increasing IED and reaction time had a positive impact on the operating cost at the range of the whole axes.

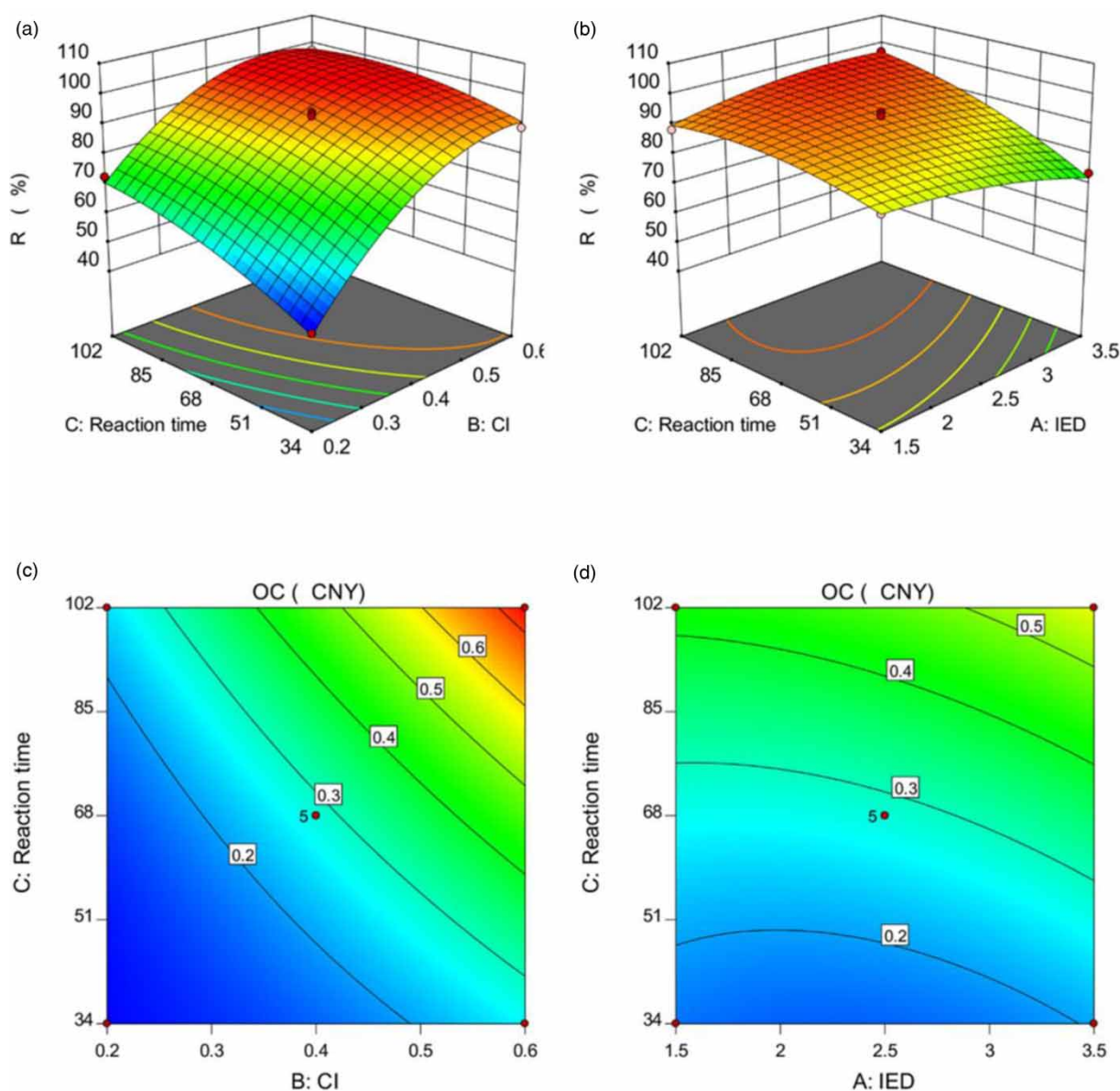


Figure 3 | 3D plot showing the effects between the EC reaction time and current intensity (a); the reaction time and inter-electrode distance (b) on phosphate removal efficiency (Y_1). Two-dimensional contour plots showing the effects between the reaction time and current intensity (c); the reaction time and inter-electrode distance (d) on operating cost (Y_2).

Optimization using desirability functions

Optimization and economic conditions were ensured at the specific point by adapting the numerical optimization of the software. To select the optimal variables for maximizing the phosphate removal efficiency and minimizing the operating cost, Derringer's desired function methodology serves as a foundation to maximize the desirability function, which is comprised of individual desirability functions of each response and a composite function based on the combination of the former, which, more often than not, is an

arithmetic or geometric mean (Costa *et al.* 2011). Finally the desirability value in this work was attained as 0.852, close to the ideal value of 1 (Makwana & Ahammed 2016).

On the basis of BBD results, the optimal conditions are disclosed in Table 6, by rounding off the values found to be the IED of 1.8 cm, CI of 0.51 A and reaction time of 34 min for EC process achieving the predicted phosphate removal efficiency and operating cost of 92.08% and 0.21 CNY/g, respectively. Confirmatory experiments (Table 6) were conducted under the optimum values in triplicate, including two conditions near the optimal parameters, and gave

Table 6 | Validation experiments and experimental values for different modes

Num	IDE	Reaction time	CI	Removal efficiency (%)			Operating cost (CNY/g)		
				Y_{exp}	Y_{pre}	Deviation	Y_{exp}	Y_{pre}	Deviation
1	1.8	34	0.51	90.24	92.08	2.0	0.22	0.21	4.5
2	1.8	34	0.48	90.16	90.61	0.5	0.21	0.20	4.8
3	1.8	34	0.55	94.12	93.29	−0.9	0.23	0.23	0
Mode		Average voltage (V)		Removal efficiency (%)			Operating cost (CNY/g)		
Switching		14.92		90.24			0.22		
Non-switching		23..40		80.14			0.35		

results of phosphate removal efficiency and operating cost of 90.24% and 0.22 CNY/g. The optimal variables gave rise the experimental data that were similar to the model prediction, with maximum $\pm 2\%$ deviation on phosphate removal efficiency and $\pm 5\%$ deviation on operating cost observed.

DISCUSSION

Through the combined biofilm and EC process, there was less than 1.0 mg/L TP in effluent, which met the first-class discharge standard (1 mg/L) of TP for rural sewage treatment facilities (DB 12/899-2019). The total iron in the effluent was 5.34 ± 2.88 mg/L. However, when ferric chloride was used to remove phosphorus, a molar ratio between iron and phosphate was typically greater than 1.5 or even higher (Asensi *et al.* 2019), meaning that at least 27 mg/L iron was added to treat the initial phosphate concentration of 10 mg/L. Therefore, the effluent total iron concentration using ferric chloride (>10 mg/L) is often higher than that in this study. It can be perceived that optimized conditions in this study are capable of yielding preferable results at a very low current intensity, to permit the ease of comparisons amongst various results, and a current intensity of 0.51 A corresponds to 2.1 mA/cm², which is sufficiently small as compared to other previous study groups (Subramanyan *et al.* 2009; Nguyen *et al.* 2014; Makwana 2017; Bakshi *et al.* 2020). This situation can be chalked up to application of the periodic switching polarity. In case of the operating cost, a value of 0.21 CNY/g P is relatively economical by contrast with that documented early for EC methods in the literature. Kobya *et al.* (2010) compared the batch and continuous EC process for treatment of rinse water. While the initial phosphate concentration was about 120 mg/L, the removal efficiency of phosphate using iron electrode materials in continuous

mode reached 85.5%–99.6% as well as the OC of 5.6–12.9 US\$/m³, and it was calculated that the corresponding OC of the unit phosphate was 0.38–0.75 CNY. Subsequently, Tran *et al.* (2012) reported that a total cost varying from 0.24 to 0.35 CAN\$/m³ was measured in the continuous-flow mode and, expressed in terms of operating cost of per unit of phosphorus, was 0.18–0.28 CNY/g. Kuokkanen *et al.* (2015) employed an EC technique in two types of real wastewater of industrial phosphate-containing mining wastewater (MWW) and dairy wastewater (DWW) and in optimum conditions, OC were calculated to be 75–80 €/kg p for MWW and 2.5 €/kg p for DWW, and those converted into RMB (exchange rate is 7.99 ¥/€) were 0.6–0.64 CNY/g and 0.02 CNY/g, respectively. The major discrepancy can be interpreted by the fact that total phosphorus concentration in MWW was roughly 5 mg/L and in comparison, that in DWW reached up to 130 mg/L. Likewise, Hashim *et al.* (2019) also drew an operating cost of 0.503 \$/m³ using a new baffle plates aluminum-based electrochemical device, which also indicated that the OC would be 0.40 CNY/g when the initial concentration was around 10 mg/L. In this study, the reason for the relatively low OC may be attributed to the use of periodic polarity switching. To elucidate this fact, we adopted the non-switching polarity mode to run under the optimal parameter conditions, and measured values for different mode are listed in Table 6. It can be seen from Table 6 that the average voltage of the non-switching polarity mode is significantly higher than that of the switching polarity. In non-switching polarity mode, there is an impermeable oxide layer on the cathode and irregular wear on the anode as well as more flocs near the anode after electrolysis, compared with uniform dissolution of both cathode and anode in the case of switching polarity mode. Distinctly, this oxide film restrains the effective current transfer, so the removal efficiency declines from

90.24% to 80.14% and the corresponding operating cost increases by 0.13 CNY/g PO_4^- . The results indicated that the use of the switching polarity mode promoted a lower OC and higher efficiency in phosphate removal under the conditions tested.

In order to further understand the influence of the switching polarity mode, physicochemical characteristics of sludge produced by EC of two modes was investigated, including X-Ray Diffraction analysis (XPS) and settling performance of sludge. XPS analysis showed the binding energy of the two modes was almost the same, which indicated there was no obvious difference in the sludge composition of the two modes. The contents of Fe, P, C and N elements were 37.79%, 2.24%, 58.24% and 1.73%, respectively, for switching polarity mode, and 40.30%, 1.88%, 55.89%, and 1.93%, respectively, for non-switching mode. The utilization ratio of iron to remove phosphate (P/Fe) of switching mode was 0.059, higher than that of 0.047 of non-switching mode. The sludge settling velocity represents the efficiency of sludge generated during EC, and its measurement could refer to the research of Ricordel & Djelal (2014). Average settling velocities (average between 5 and 30 min settling) were 0.088 L/min for switching mode and 0.080 L/min for non-switching mode, demonstrating that sludge of switching mode was denser and more easily dewatered.

However, from another perspective, this OC value showed the disadvantage over the chemical treatment such as using ferric chloride. Two deficiencies raised the cost of EC: one was the relatively low initial phosphate concentration increasing the operating cost of unit phosphorus removal; the other one was the combination of EC and biological process, making these two into one integrated treatment system, which entailed a longer duration to ensure that the denitrification efficiency would not be affected. Considering the operating cost of unit phosphorus removal, EC technique is more suitable for higher phosphate concentration than chemical processes, since it can adapt to a larger fluctuation range of phosphorus concentration and still maintains a considerable removal rate when the phosphorus concentration is very high (Tran *et al.* 2012). In addition, another significant advantage of EC is that the residual Fe concentration was lower at the end of treating effluent. This advantage greatly alleviates the costs associated with chemical transportation because EC itself produces in-situ coagulants and does not require supererogatory neutralization against chemical treatment. In brief, the combination of biofilm system and EC step demonstrates a promising option for enhancing phosphate removal, but combining biological

and EC processes in one integrated treatment system might cause a defect in operating cost, since the mutual effect of the two process parameters requires to be taken into account, such as reaction time and phosphate concentration. Therefore, some recommendations are supplied for further reducing the operating cost of the combined system. (i) A semi-continuous flow mode is suggested to be applied in the combined biological treatment and EC system, especially for relatively low initial phosphate concentration, which means that previously biologically treated effluents enter the EC process intermittently and in this way the reaction time of two processes can be separately controlled. (ii) Electrode material is not merely limited to iron or aluminum electrodes, so it is a requisite issue to explore new electrodes and electrode array modes to signal lower phosphate level at a lower current density. (iii) Mono- or bipolar and other combinations of electrode arrangement should be further optimized.

CONCLUSIONS

The combination of EC process and biofilm treatment to reinforce phosphorus removal was investigated in a lab-scale study. The application of a three-factor, three-level Box-Behnken design assisted in obtaining a desirable solution for maximizing phosphate removal efficiency with the support of minimizing operating cost. Also, the adaptability of the developed mathematical model was critically provided by different statistical analyses. Predicted values obtained with quadratic equations were in remarkable agreement with the experimental values. The optimal parameters were found to be inter-electrode distance of 1.8 cm, current density of 0.51 A (2.1 mA/cm^2) and EC reaction time of 34 min. Under these conditions, a phosphate removal efficiency of 90.24% was achieved and effluent phosphate was less than 1 mg/L. A higher efficiency and lower OC in phosphate removal were principally attributed to the use of periodic switching polarity mode. The integrated biofilm system followed by EC can be a better option for wastewater containing higher P concentration with not merely tech-economy but also other merits. To sum up, these results indicate that combining electrocoagulation with biological process is a feasible and effective method for enhancing phosphate removal and also provides more references for the integrated system of combination of biological treatment and EC polishing step.

ACKNOWLEDGEMENTS

This work was supported by the National Key R&D Program of China (Grant No. 2018YFE0106400).

DATA AVAILABILITY STATEMENT

All relevant data are included in the paper or its Supplementary Information.

REFERENCES

- Abbasi, S., Mirghorayshi, M., Zinadini, S. & Zinatizadeh, A. A. 2020 A novel single continuous electrocoagulation process for treatment of licorice processing wastewater: optimization of operating factors using RSM. *Process Safety and Environmental Protection* **134**, 323–332.
- Acharya, S., Sharma, S. K., Chauhan, G. & Shree, D. 2018 Statistical optimization of electrocoagulation process for removal of nitrates using response surface methodology. *Indian Chemical Engineer* **60**, 269–284.
- Almeida, B. M., Erthal, S. R., Padua, O. E., Silveira, V. L. & Amélia, E. L. 2008 Response surface methodology (RSM) as a tool for optimization in analytical chemistry. *Talanta* **76** (5), 965–977.
- Amour, A., Merzouk, B., Leclerc, J. P. & Lapicque, F. 2015 Removal of reactive textile dye from aqueous solutions by electrocoagulation in a continuous cell. *Desalination and Water Treatment* **57**, 48–49.
- APHA, AWWA, WPCF 1999 *Standard Methods for the Examination of Water and Wastewater*, 20th edn. American Public Health Association, Washington.
- Asensi, E., Alemany, E., Duque-Sarango, P. & Aguado, D. 2019 Assessment and modelling of the effect of precipitated ferric chloride addition on the activated sludge settling properties. *Chemical Engineering Research and Design* **150**, 14–25.
- Attour, A., Touati, M., Tlili, M., Amor, M. B., Lapicque, F. & Leclerc, J. P. 2014 Influence of operating parameters on phosphate removal from water by electrocoagulation using aluminum electrodes. *Separation and Purification Technology* **123**, 124–129.
- Bakshi, A., Verma, A. K. & Dash, A. K. 2020 Electrocoagulation for removal of phosphate from aqueous solution: statistical modeling and techno-economic study. *Journal of Cleaner Production* **246**, 1–13.
- Bouwman, A. F., Beusen, A. H. W. & Billen, G. 2009 Human alteration of the global nitrogen and phosphorus soil balances for the period 1970–2050. *Global Biogeochemical Cycles* **23**, 1–16.
- Buzzini, A. P., Patrizzi, L. J., Motheo, A. J. & Pires, E. C. 2007 Preliminary evaluation of the electrochemical and chemical coagulation processes in the post-treatment of effluent from an upflow anaerobic sludge blanket (UASB) reactor. *Journal of Environmental Management* **85** (4), 847–857.
- Castañeda, L. F., Coreño, O. & Nava, J. L. 2020 Simultaneous elimination of hydrated silica, arsenic and phosphates from real groundwater by electrocoagulation using a cascade-shaped up-flow reactor. *Electrochimica Acta* **331**, 1–8.
- Chauhan, G. 2013 Development of green technology for extraction of nickel from spent catalyst and its optimization using response surface methodology. *Green Processing and Synthesis* **2**, 259–271.
- Costa, N. R., Lourenço, J. & Pereira, Z. L. 2011 Desirability function approach: a review and performance evaluation in adverse conditions. *Chemometrics and Intelligent Laboratory Systems* **107** (2), 234–244.
- Damaraju, M., Bhattacharyya, D. & Kurilla K, K. 2017 Removal of recalcitrant carbon from an industrial wastewater using electrocoagulation. *International Journal of Civil Engineering* **15** (4), 1–7.
- Daneshvar, N., Oladegaragoze, A. & Djafarzadeh, N. 2006 Decolorization of basic dye solutions by electrocoagulation: an investigation of the effect of operational parameters. *Journal of Hazardous Materials* **129** (1), 116–122.
- Demim, S., Drouiche, N., Aouabed, A., Benayad, T., Couderchet, M. & Semsari, S. 2014 Study of heavy metal removal from heavy metal mixture using the CCD method. *Journal of Industrial and Engineering Chemistry* **20** (2), 512–520.
- Dura, A. & Breslin, C. B. 2019a Electrocoagulation using stainless steel anodes: simultaneous removal of phosphates, Orange II and zinc ions. *Journal of Hazardous Materials* **374**, 152–158.
- Dura, A. & Breslin, C. B. 2019b The removal of phosphates using electrocoagulation with Al–Mg anodes. *Journal of Electroanalytical Chemistry* **846**, 1–8.
- Garg, K. K. & Prasad, B. 2016 Development of Box Behnken design for treatment of terephthalic acid wastewater by electrocoagulation process: optimization of process and analysis of sludge. *Journal of Environmental Chemical Engineering* **4**, 178–190.
- Hakizimana, J. N., Gourich, B., Chafi, M., Stiriba, Y., Vial, C., Drogui, P. & Naja, J. 2017 Electrocoagulation process in water treatment: a review of electrocoagulation modeling approaches. *Desalination* **404**, 1–21.
- Hashim, K. S., Khaddar, R. A., Jasim, N., Shaw, A., Phipps, D., Kot, P., Pedrola, M. O., Alattabi, A. W., Abdulredha, M. & Alawsh, R. 2019 Electrocoagulation as a green technology for phosphate removal from river water. *Separation and Purification Technology* **210**, 135–144.
- Hosni, K., Moussa, S. B. & Amor, M. B. 2006 Conditions influencing the removal of phosphate from synthetic wastewater: influence of the ionic composition. *Desalination* **206**, 279–286.
- Jensen, W. A. 2017 Response surface methodology: process and product optimization using designed experiments. *Journal of Quality Technology* **49**, 186–188.
- Kabuk, H. A., İlhan, F., Avsar, Y., Kurt, U., Apaydin, O. & Gonullu, M. T. 2014 Investigation of leachate treatment with electrocoagulation and optimization by response surface methodology. *Clean Soil, Air, Water* **42**, 571–577.

- Koby, M., Demirbas, E., Dedeli, A. & Sensoy, M. T. 2010 Treatment of rinse water from zinc phosphate coating by batch and continuous electrocoagulation processes. *Journal of Hazardous Materials* **173** (1–3), 326–334.
- Kuokkanen, V., Kuokkanen, T., Rämö, J., Lassi, U. & Roininen, J. 2015 Removal of phosphate from wastewaters for further utilization using electrocoagulation with hybrid electrodes – techno-economic studies. *Journal of Water Process Engineering* **8**, E50–E57.
- Makwana, A. 2017 Effect of 2D electrocoagulation on phosphate removal from UASBR treated sewage. *Journal of Engineering Sciences and Research Technology* **6**, 785–791.
- Makwana, A. R. & Ahammed, M. M. 2016 Continuous electrocoagulation process for the post-treatment of anaerobically treated municipal wastewater. *Process Safety and Environmental Protection* **102**, 724–733.
- Maran, J. P., Sivakumar, V., Thirugnanasambandham, K. & Sridar, R. 2014 Model development and process optimization for solvent extraction of polyphenols from red grapes using Box-Behnken design. *Preparative Biochemistry and Biotechnology* **44**, 56–57.
- Nguyen, D. D., Kim, S. D. & Yoon, Y. S. 2014 Enhanced phosphorus and COD removals for retrofit of existing sewage treatment by electrocoagulation process with cylindrical aluminum electrodes. *Desalination and Water Treatment* **52** (13–15), 2388–2399.
- Ricordel, C. & Djelal, H. 2014 Treatment of landfill leachate with high proportion of refractory materials by electrocoagulation: system performances and sludge settling characteristics. *Journal of Environmental Chemical Engineering* **2** (3), 1551–1557.
- Shonza, N. S., Andreatta, D., Muniz, E. P., Dalmascio, C. J., de Freitas, R. R. & da Silva Porto, P. S. 2020 Crude oil wastewater treatment by electrocoagulation in a continuous process with polarity switch. *Environmental Technology*. doi: 10.1080/09593330.2020.1847205.
- Subramanyan, V., Jothinathan, L., Jeganathan, J. & Ganapathy, S. 2009 Remediation of phosphate-contaminated water by electrocoagulation with aluminium, aluminium alloy and mild steel anodes. *Journal of Hazardous Materials* **164** (2–3), 1480–1486.
- Tak, B. Y., Tak, B. S., Kim, Y. J., Park, Y. J., Yoon, Y. H. & Min, G. H. 2015 Optimization of color and COD removal from livestock wastewater by electrocoagulation process: application of Box-Behnken design (BBD). *Journal of Industrial and Engineering Chemistry* **28**, 307–315.
- Tran, N., Drogui, P., Blais, J. F. & Mercier, G. 2012 Phosphorus removal from spiked municipal wastewater using either electrochemical coagulation or chemical coagulation as tertiary treatment. *Separation and Purification Technology* **95**, 16–25.
- Xiangyong, Z., Hainan, K., Deyi, W., Chong, W., Yan, L. & Hairen, Y. 2009 Phosphate removal from source separated urine by electrocoagulation using iron plate electrodes. *Water Science and Technology* **60** (11), 2929–2938.
- Yong, Z. Z., Yin, X. H., Pei, S. P., Hui, Z. Y. & Feng, Z. 2015 Application of electrocoagulation in water treatment. *Modern Chemical Industry* **35** (4), 29–32 and 34.
- Zhang, S., Zhang, J., Wang, W., Li, F. & Cheng, X. 2013 Removal of phosphate from landscape water using an electrocoagulation process powered directly by photovoltaic solar modules. *Solar Energy Materials and Solar Cells* **117**, 73–80.

First received 9 October 2020; accepted in revised form 24 March 2021. Available online 5 April 2021